# Giant tunnel electroresistance in ferroelectric tunnel junctions with metal contacts to two-dimensional ferroelectric materials

Lili Kang,[1,2] Peng Jiang [1,2] Hua Hao,[1] Yanhong Zhou,[3] Xiaohong Zheng,[1,2,*] Lei Zhang,[4,5,†] and Zhi Zeng[1]

[1]*Key Laboratory of Materials Physics, Institute of Solid State Physics, HFIPS, Chinese Academy of Sciences, Hefei 230031, China*
[2]*Science Island Branch of Graduate School, University of Science and Technology of China, Hefei 230026, China*
[3]*College of Science, East China Jiao Tong University, Nanchang, Jiangxi 330013, China*
[4]*State Key Laboratory of Quantum Optics and Quantum Optics Devices, Institute of Laser Spectroscopy,*
*Shanxi University, Taiyuan 030006, China*
[5]*Collaborative Innovation Center of Extreme Optics, Shanxi University, Taiyuan 030006, China*

Two-dimensional (2D) ferroelectric materials (FEMs) and their application in ferroelectric tunnel junctions (FTJs) have attracted a great deal of attention during the past several years due to their great potential in nonvolatile memory devices. Particularly, the all-2D FTJs, which have only atomic-layer thickness, have been demonstrated to show very high tunnel electroresistance (TER) ratio. Nevertheless, to better integrate with the present semiconductor technology, it is necessary to consider metal contacts in the construction of FTJs with 2D FEMs. However, due to the unknown interaction between traditional metals and 2D FEMs, it is not clear whether ferroelectricity still persists when the 2D FEMS are in contact with metals and whether the corresponding FTJs exhibit high TER effect as demanded for memory devices. To probe this, we construct FTJs with top contact between Au(010) and $In_2Se_3$, a 2D FEM with out-of-plane ferroelectric polarization. By density functional calculations combined with a nonequilibrium Green function technique, we find that not only the ferroelectricity still persists in the metal/FEM contact, but also a giant TER ratio as high as $10^4\%$ is achieved. The giant TER arises from the change of the metal/FEM contact from a Schottky type to an Ohmic type accompanying with the ferroelectric polarization reversal. In the meantime, the tunnel barrier height between Au(010) and $In_2Se_3$ is zero, which means good ability of electron injection from metal to semiconductor and low contact resistance. Our study suggests that, by properly selecting the metal materials, giant TER ratio and high performance can be achieved in FTJs constructed with 2D FEMs and metal contacts.

## I. INTRODUCTION

Ferroelectric tunnel junctions (FTJs) as a new generation of nonvolatile memory devices have attracted a great deal of attention in the past decades [1–5]. Since a FTJ writes or reads data only through an applied electric field, it has great advantages of fast speed, low-energy consumption, and noncontact operation. By far, most attention has been paid to the three-dimensional (3D) FTJs in which ferroelectric materials (FEMs) with a perovskite-type oxide structure such as $BaTiO_3$ and $PbTiO_3$ are chosen as the tunnel barrier [6–11]. A large number of strategies have been proposed to achieve very large tunnel electroresistance (TER) ratio in traditional FTJs [12–16]. However, 3D FEMs tend to lose their ferroelectricity below a critical thickness because of the charge accumulation on the surface [17,18]. This greatly limits its development because it is in contradiction with the trend of ongoing device miniaturization. Thus, new FEMs not subject to the thickness limit problem are greatly anticipated.

In recent years, two-dimensional (2D) FEMs with atomic-layer thickness have started to catch intensive attention, and many new 2D FEMs, such as group-IV monochalcogenides and $III_2$-$VI_3$ van der Waals materials, have been theoretically predicted or experimentally fabricated [19–25]. It adds a strong possibility to overcome the challenge confronted in the critical thickness in traditional FTJs. In fact, very large TERs have been reported in all-2D FTJs constructed with 2D FEMs and other 2D materials [26–28], suggesting the great potential of 2D FEMs in ferroelectric storage. Nevertheless, to better integrate with existing semiconductor technology, the metal-semiconductor-metal structure will be inevitable in real applications. Thus, practically, we need to consider bulk metal in the leads. However, since the unknown interaction between metals and FEMs is generally much more complex than that between two 2D materials which is basically of a van der Waals interaction type, it is not clear yet whether the ferroelectricity of the FEMs will still persist after contact with the 3D metals and whether large TER is achievable in the FTJs.

As a matter of fact, metal contacts to 2D materials have always been the focus of numerous studies since they are directly related to the performance of the corresponding devices based on 2D materials. Among the most frequently studied

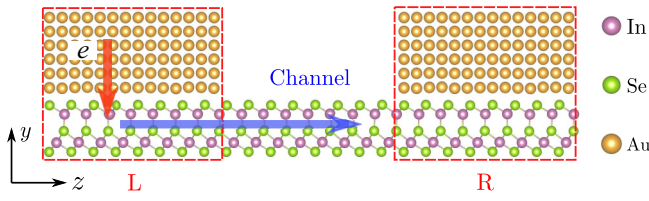*xhzheng@theory.issp.ac.cn
†zhanglei@sxu.edu.cn

FIG. 1. The structure of the FTJ. The left (*L*) and right (*R*) leads indicated by the dashed line boxes are the Au(010)-In$_2$Se$_3$ contact while the channel region is 2D In$_2$Se$_3$ layer only. The red arrow indicates the election injection process from Au(010) into In$_2$Se$_3$ and the blue arrow indicates the process of electron transmitting from the left lead into the channel region.

are the metal contacts to 2D transition-metal dichalcogenides (TMDs) [29–34]. One of the main objectives of these studies is to form low-resistance Ohmic contact for high performance in 2D materials based electronic devices. However, according to the Schottky theory, an Ohmic contact can be formed only between two materials with very large difference in their work functions [35,36]. Thus, most metal contacts are of the Schottky type, which is detrimental to achieving low-resistance contact. The metal contacts to 2D FEMs with out-of-plane ferroelectric polarization will be more complex since such FEMs have two inequivalent surfaces with different work functions. A natural question is as follows: What contact types will be formed when we bring such a FEM and metal into contact and whether they are beneficial for achieving large TER ratio in FTJs?

To get an answer to the question above, in this work, by taking 2D ferroelectric In$_2$Se$_3$ with out-of-plane ferroelectric polarization [24,25] as an example, we construct FTJs with top contact between Au(010) and In$_2$Se$_3$ as the leads and pristine In$_2$Se$_3$ as the channel region. Interestingly, it is found that the ferroelectricity still persists in In$_2$Se$_3$. Furthermore, the contact between Au and In$_2$Se$_3$ can either be Schottky type or Ohmic type, depending on whether the direction of polarization of In$_2$Se$_3$ is towards or away from the bulk Au. Such a duality of contact type arises from the big difference of the work functions between the two sides of In$_2$Se$_3$. As a result from the switching between the Schottky contact and Ohmic contact with the reverse of the ferroelectric polarization induced by the external electric field, the FTJ presents a giant TER ratio larger than $10^4$%, suggesting the great potential of metal contacts to 2D out-of-plane ferroelectric materials in nonvolatile memory devices.

## II. STRUCTURE AND COMPUTATION DETAILS

The structure of the FTJ is shown in Fig. 1, where the pristine In$_2$Se$_3$ lying in the *xz* plane is chosen as the channel region and the top contact of Au(010) and In$_2$Se$_3$ as the leads, the most common contact geometry that has been studied frequently for many other 2D materials based devices [31,37,38]. The lattice constants of Au(010) in the *xz* plane are 4.08 Å×4.08 Å and the size of rectangular unit cell of In$_2$Se$_3$ is 4.106 Å×7.11 Å. Therefore, we choose 1×7 Au unit cells and 1×4 In$_2$Se$_3$ unit cells in the *xz* plane as the supercell of the leads. This way, the lattice mismatch between the two

materials is only 0.6% and 0.42% in the *x* and *z* directions. In the *y* direction, we adopt six layers of Au atoms because the obtained results do not change appreciably beyond this thickness [39]. The periodic slabs along the *y* direction are separated by a 16-Å-thick vacuum region and dipole correction is used to remove the artificial potential drop between neighboring supercells which is prominent in slab polar materials due to the periodic boundary condition imposed in the calculations [40].

The geometry relaxation and electronic structure calculations are performed using the Vienna *ab initio* simulation package (VASP) [41,42], which is based on density functional theory (DFT) using the projector-augmented wave method and a plane-wave basis set [43]. The exchange-correlation potential takes the form of Perdew-Burke-Ernzerhof (PBE) in the generalized gradient approximation (GGA) [44]. The energy cutoff is set to be 250 eV. In the atomic structure relaxation, the van der Waals (vdW) interaction is taken into consideration by the DFT-D2 method [45]. The *k*-point sampling grid is chosen as 12×1×2. The structures are deemed fully relaxed when the Hellmann-Feynman force gets below the tolerance 0.05 eV/Å and the electronic energy difference between two consecutive steps gets below $10^{-3}$ eV.

The calculations of quantum transport are performed by the TRANSIESTA method [46,47], which combines the density functional theory (DFT) and the nonequilibrium Green's function (NEGF) technique for the study of open systems and is included in the SIESTA package [48,49]. The generalized gradient approximation (GGA) with form of Perdew-Burke-Ernzerhof (PBE) [44] is applied for the exchange-correlation potential. The cutoff energy is set to be 500 Ry in our case. The basis type is double zeta basis plus polarization (DZP) and the *k*-point mesh is chosen as 15×1×1 for the self-consistent (SC) calculation of the central scattering region. The transmission function is calculated by the TBTRANS code and the *k*-point mesh is chosen as 100×1×1 because the *k*-point number needs to be much larger for convergence in transmission calculation. The tunneling conductance as a function of electron energy *E* is obtained by the formula

$$G(E) = \frac{2e^2}{h} T(E), \qquad (1)$$

where $T(E) = \sum_{k_\parallel} T(k_\parallel, E)$ is the *k*-point averaged transmission function at energy *E* and $T(k_\parallel, E)$ is the *k* resolved transmission function with $k_\parallel = k_x$. The TER ratio is defined as

$$R = \frac{|G_\uparrow - G_\downarrow|}{\min(G_\uparrow, G_\downarrow)}, \qquad (2)$$

where $G_\uparrow$ and $G_\downarrow$ are the tunneling conductances of the FTJ when the ferroelectric layer is in the up-polarized ($P_\uparrow$) state and in the down-polarized ($P_\downarrow$) state, respectively.

## III. RESULTS AND DISCUSSION

We first investigate the geometry structures of the contact between the ferroelectric In$_2$Se$_3$ and Au(010) and the change of the electrical polarization of the In$_2$Se$_3$ when it is in contact with Au(010). In the structure relaxation, four top Au atomic layers are fixed and all other atomic layers including
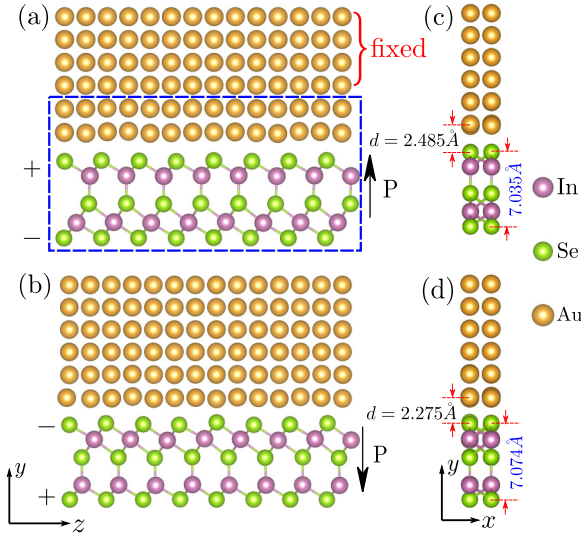
FIG. 2. The geometry structures for (a) the $P_\uparrow$ case and (b) the $P_\downarrow$ case. The relaxed contact distance and layer thickness of In$_2$Se$_3$ in the $P_\uparrow$ and $P_\downarrow$ cases are presented in (c) and (d), respectively. The plus and minus signs indicate the positively and negatively charged surfaces, respectively.

two Au layers and the In$_2$Se$_3$ are allowed to move freely [see Fig. 2(a)]. To determine the most energetically favorable configuration, we shift the In$_2$Se$_3$ layer relative to the Au layer in the $xz$ plane and considered six cases as shown in Fig. 3(a). The top view and side view of case 1 are shown in Figs. 3(b) and 3(c), respectively. In the supercell of this
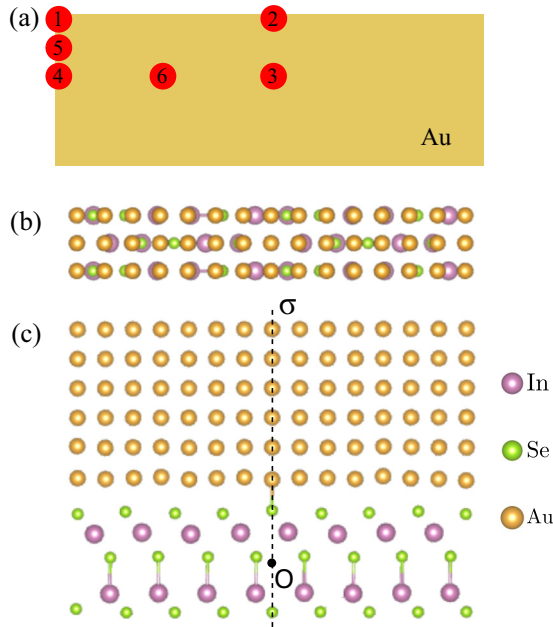


FIG. 3. (a) The six configurations with relative shift of the In$_2$Se$_3$ by (1) (0.0,0.0); (2) (0.5,0.0); (3) (0.5,0.5); (4) (0.0,0.5); (5) (0.0,0.25); and (6) (0.25,0.5) in units of lattice constants in the $x$ and $z$ directions, respectively. (b) The top view of case 1; (c) the side view of case 1. $\sigma$ is the symmetry plane while $O$ is the inversion center for the two In layers and the top and bottom Se layers.

TABLE I. The energy of the six configurations as shown in Fig. 3(a). All the energies are relative to that of case 1.

| Case | 1 | 2 | 3 | 4 | 5 | 6 |
|---|---|---|---|---|---|---|
| Energy (eV) | 0.00 | 0.31 | 1.15 | 0.37 | 0.08 | 0.17 |

case, the Au atoms are symmetrically distributed around the central vertical $\sigma$ plane. In the meantime, the top and bottom Se layers and the two In layers are centrosymmetrical in the local In$_2$Se$_3$ system, with the local inversion center $O$ located at the $\sigma$ plane. The atoms in the inner Se layer will move to the other side of the inversion center $O$ with the reversal of the ferroelectric polarization. The other cases are obtained by shifting the In$_2$Se$_3$ supercell to the specified position as shown in Fig. 3(a). After full relaxation, the energies of these cases are shown in Table I. It is found that case 1 is the most energetically favorable configuration. Thus, all the following studies are based on it.

For the two initial $P_\uparrow$ and $P_\downarrow$ configurations of In$_2$Se$_3$, the fully relaxed structures are presented in Figs. 2(a) and 2(b) and the contact distances between Au and In$_2$Se$_3$ are obtained as 2.485 and 2.275 Å, respectively [see Figs. 2(c) and 2(d)]. In addition, the thickness of In$_2$Se$_3$ as measured by the distance between the top and bottom Se atoms is increased to 7.035 and 7.074 Å for the $P_\uparrow$ and $P_\downarrow$ cases, respectively, as compared with 6.785 Å of the freestanding In$_2$Se$_3$. Accordingly, the final electrical polarization strengths in both structures are obtained as 0.123 $e$ Å/unit cell and 0.083 $e$ Å/unit cell, respectively. Note that the electrical polarizations obtained above are for the whole contact structures. In contrast, the electrical polarization of freestanding In$_2$Se$_3$ is 0.094 $e$ Å/unit cell. Thus, the two polarization states still persist in the contact structure. To evaluate the energy barrier during the polarization switching, we have set a path from the initial state to the final state by linear interpolation. By comparing the energy of all the configurations, we obtained the energy barrier as 0.98 eV per unit cell of In$_2$Se$_3$.

Next, we investigate the electrical behaviors of the FTJ as shown in Fig. 1, in which the leads are the In$_2$Se$_3$-Au(010) hybrid structure, while the channel region is In$_2$Se$_3$ only. When the device is in work, the electrons should first enter the semiconducting In$_2$Se$_3$ from the top gold metal in the lead (we call it process 1) and then transmit into the channel region (process 2), as indicated by the red and blue arrows in Fig. 1. Thus, to have a good performance, the FTJ should be in a good condition in at least two aspects. First, it should be easy for the electrons to be injected from the metal into the semiconductor. This is extremely important for the high performance of all metal-semiconductor contacts since high electron injection ability is generally accompanied with low contact resistance, which is still a challenge to achieve at present [29–31]. Second, as a memory device, we should have a large TER ratio.

The ability of electron injection can be evaluated by the tunnel barrier between the bulk gold and the In$_2$Se$_3$ layer. The barrier width $d$ as shown in Figs. 4(a) and 4(b) is defined as the width of vdW gap between Au and In$_2$Se$_3$. According to the above results of structural optimization, $d$ is 2.485
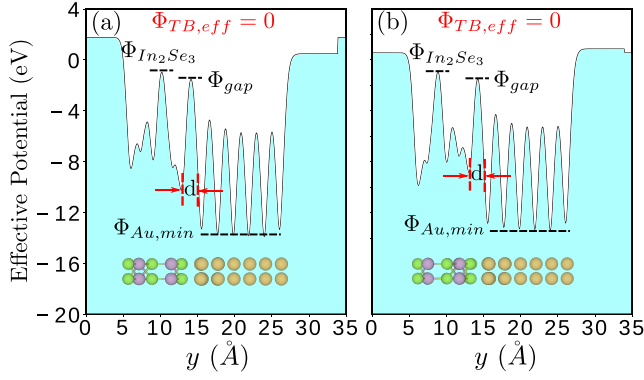
FIG. 4. The effective potential ($V_{\text{eff}}$) along the $y$ direction (the direction perpendicular to the interface) of Au-In$_2$Se$_3$ contact system for (a) $P_\uparrow$ and (b) $P_\downarrow$. $\Phi_{\text{In}_2\text{Se}_3}$, $\Phi_{\text{gap}}$, and $\Phi_{\text{Au,min}}$ are the $V_{\text{eff}}$ of In$_2$Se$_3$, the van der Waals (vdW) gap between Au and In$_2$Se$_3$ layer, and the minimum $V_{\text{eff}}$ of Au, respectively. $\Phi_{\text{TB,eff}}$ is the tunnel barrier height. $d$ is the width of vdW gap between Au and In$_2$Se$_3$.

and 2.275 Å for the $P_\uparrow$ case and the $P_\downarrow$ case, respectively. The tunnel barrier height is labeled as $\Phi_{\text{TB,eff}}$, which is the minimum barrier height that an electron has to overcome when it transmits from the metal to the semiconductor. The tunnel barrier height is evaluated by the effective potential along the $y$ direction (the direction perpendicular to the interface). Figures 4(a) and 4(b) present the effective potential for the $P_\uparrow$ and $P_\downarrow$ cases, respectively, as obtained by the SIESTA code. According to the method for calculating tunnel barrier height($\Phi_{\text{TB,eff}}$) in the literatures [29,32], we have

$$\Phi_{\text{TB,eff}} = \begin{cases} \Phi_{\text{gap}} - \Phi_{sc}, & \Phi_{\text{gap}} > \Phi_{sc} > \Phi_{\text{metal,min}} \\ \Phi_{\text{gap}} - \Phi_{\text{metal,min}}, & \Phi_{\text{gap}} > \Phi_{\text{metal,min}} > \Phi_{sc} \\ 0, & \Phi_{sc} \geqslant \Phi_{\text{gap}} \\ 0, & \Phi_{\text{metal,min}} \geqslant \Phi_{\text{gap}} \end{cases} \quad (3)$$

where $\Phi_{sc}$, $\Phi_{\text{gap}}$, and $\Phi_{\text{metal,min}}$ are, respectively, the maximum value of the 2D semiconductor, the value of the van der Waals (vdW) gap between 2D semiconductor and metal, and the minimum value of the metal of the effective potential of the whole device. Applying the above formula to our case, we find from Figs. 4(a) and 4(b) that the effective potential of In$_2$Se$_3$ ($\Phi_{\text{In}_2\text{Se}_3}$) is higher than the effective potential of van der Waals (vdW) gap between Au and In$_2$Se$_3$ layer ($\Phi_{\text{gap}}$) for both the $P_\uparrow$ and $P_\downarrow$ cases. It means that the $\Phi_{\text{TB,eff}}$ is zero for both polarization states, which indicates high electron injection efficiency and thus low contact resistance in this FTJ. This is beneficial for the design of energy-saving devices.

Then, the difference in the equilibrium conductance of the FTJ arising from the reversal of the ferroelectric polarization is studied. The transmission functions at zero bias for the two cases of $P_\uparrow$ and $P_\downarrow$ are given in Fig. 5(a). We find that the transmission in the $P_\downarrow$ state is more than two orders of magnitude larger than that in the $P_\uparrow$ state around the $E_F$. With the transmission function, we can obtain the tunneling conductance by Eq. (1) and further the TER ratio by Eq. (2). The TER ratio as a function of the electron energy is shown in Fig. 5(b). It is found that the TER ratio around the $E_F$ is larger
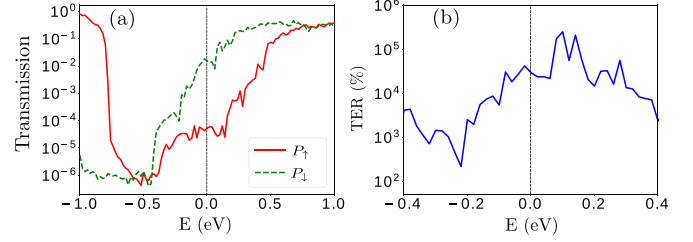


FIG. 5. (a) The transmission functions for both polarized states; (b) the TER ratio as a function of electron energy.

than $10^4$%, which suggests very large electrical response with the reversal of the ferroelectric polarization and is comparable to those of the previously reported all-2D FTJs [26–28]. However, we note that the TER ratio in the presented configuration may not be the maximum. When both Au-In$_2$Se$_3$ interfaces are metallic, their electron density spreads and may overlap when the two Au leads are close enough. No such effect exists for the semiconducting interfaces. Thus, an even larger resistance ratio may be obtained if Au leads are close enough to each other.

To reveal the origin for the large TER ratio obtained, we start with the analysis of contact type of the interfaces. There are two kinds of interfaces in the junction: one lying between Au and In$_2$Se$_3$ inside the lead region, and the other separating the lead region (Au-In$_2$Se$_3$ hybrid structure) and the channel region (In$_2$Se$_3$). First of all, we analyze the first kind of interface. Figures 6(a)–6(c) show the PDOS contributions of In atoms and Se atoms of pristine In$_2$Se$_3$ without contact and those of Au-In$_2$Se$_3$ contact system inside the lead region for $P_\uparrow$ and $P_\downarrow$, respectively. It is obvious that the pristine In$_2$Se$_3$ is a semiconductor with an energy gap of about 1 eV, which is consistent with previous study [24]. When it is in contact with Au with upward polarization, due to the hybridization between Au and In$_2$Se$_3$, metal-induced gap states [50] can be clearly observed [compare Figs. 6(a) and 6(b)]. In the meantime, the Fermi level ($E_F$) has a little shift towards the conduction band compared with the pristine In$_2$Se$_3$, but still in the energy gap. This illustrates that the contact between Au and In$_2$Se$_3$ with upward polarization is an $n$-type Schottky contact. In contrast, the type of contact between Au and In$_2$Se$_3$ becomes Ohmic when the direction of polarization of In$_2$Se$_3$ is reversed to $P_\downarrow$. As shown in Fig. 6(c), the $E_F$ of In$_2$Se$_3$ lies in its conduction band, which indicates that In$_2$Se$_3$ with downward polarization is metallic when it contacts Au.

The positions of the Fermi level relative to the bands of In$_2$Se$_3$ in the contact structures can be understood from two factors: one is the Fermi level pinning effect [51,52] and the other is the charge transfer effect between the In$_2$Se$_3$ and Au for the two polarization states due to the differences in work functions of Au and In$_2$Se$_3$ as shown in Fig. 6(f). The plus and minus signs marked on the figure are the positively and negatively charged sides of In$_2$Se$_3$. The work function is computed as $W = E_0 - E_F$, where $E_F$ is the Fermi level and $E_0$ is the vacuum level, corresponding to the effective potential at the vacuum layer in our calculations. Although for semiconductors, there is no well-defined Fermi level, a routine is to take it at the middle gap or at the valence band
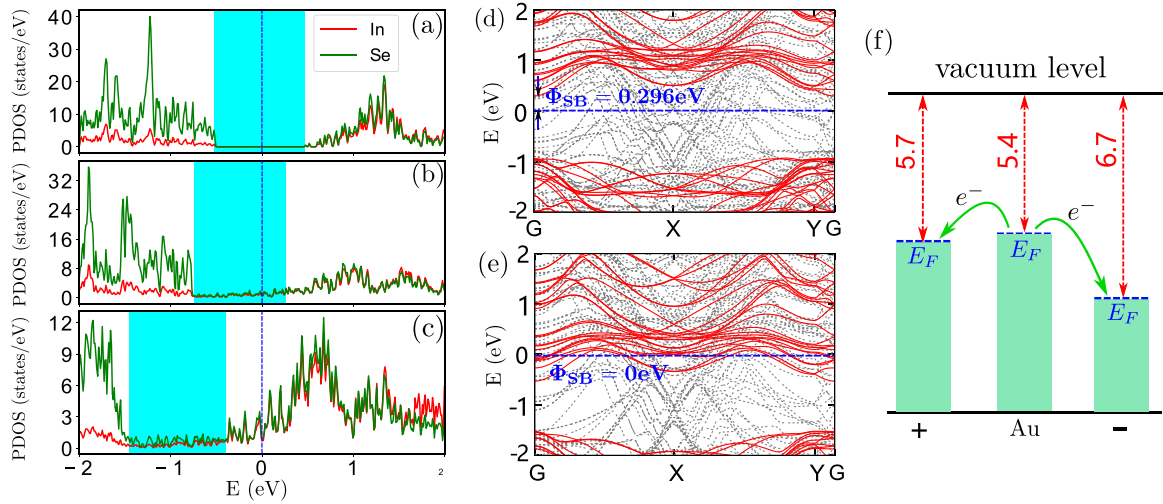
FIG. 6. PDOS of Au contacts to $In_2Se_3$: (a) the contributions of In atoms and Se atoms of pristine $In_2Se_3$. (b), (c) The contributions of In atoms and Se atoms of the Au-$In_2Se_3$ contact system in the $P_\uparrow$ and $P_\downarrow$ cases, respectively. The blue shadow indicates the energy gap of $In_2Se_3$ for these three cases. The band structures of Au-$In_2Se_3$ system are plotted for the cases (d) $P_\uparrow$ and (f) $P_\downarrow$, in which the red solid lines indicate the band structure of pristine $In_2Se_3$. The Schottky barrier ($\Phi_{SB}$) is marked in blue. (f) The work functions and schematic diagram indicating the direction of possible charge transfer between Au and $In_2Se_3$, where plus and minus signs stand for the positively and negatively charged sides of $In_2Se_3$, respectively, as shown in Fig. 2.

maximum (VBM), just as done in the references (see, e.g., Ref. [53]). Since we consider zero temperature and no impurity levels in the gap, we calculate the work function by taking the Fermi level as VBM. It is reasonable since the work function measures the energy difference between the vacuum level and the highest energy level of filled electrons. It is found that the work functions of the two sides of $In_2Se_3$ are different because of its nonsymmetric structure and the subsequent built-in electrical field induced by the spontaneous ferroelectric polarization along the vertical direction, with that (5.70 eV) of the "+" side slightly higher than that (5.40 eV) of Au(010) and that (6.70 eV) of the "−" side much larger than that of Au(010). It is well known that electrons will transfer from the lower work function side to the higher work function side when two materials are brought into contact and the magnitude of the electron transfer depends on the difference between the two work functions [54]. Thus, electrons will transfer from Au(010) to $In_2Se_3$ when it contacts by the "+" side (the $P_\uparrow$ case), but the magnitude of the electron transfer will be very small due to the almost equal work functions of the two materials, with the difference as small as 0.3 eV. This very small electron transfer would shift the Fermi level to the bottom of the conduction band of $In_2Se_3$. However, we see that the Fermi level still lies deep in the band gap. This originates from Fermi level pinning effect due to the metal-induced gap states and this effect plays the dominant role. In contrast, when the "−" side of $In_2Se_3$ is in contact with Au(010) (the $P_\downarrow$ case), the difference between work functions of the two materials is much larger (∼1.0 eV), thus electron transfer will be much larger and the electrons move from the Au(010) to $In_2Se_3$, which shifts the Fermi level to the conduction band of $In_2Se_3$. Obviously, in this case, the Fermi level pinning effect plays a minor role, compared with the large charge transfer. This well explains why the $In_2Se_3$ in the $P_\uparrow$ state is still a semiconductor but that in the $P_\downarrow$ state is metallic, as shown in Figs. 6(b) and 6(c).

Next, we analyze the second kind of interface. The band structures of two polarization states of the leads and that of the pristine $In_2Se_3$ (channel region) are shown in Figs. 6(d) and 6(e) as gray dashed lines and red solid lines, respectively. The pristine $In_2Se_3$ band structure is superimposed on the band structure of Au-$In_2Se_3$ contact system in such a way that the valence band maxima of the pristine $In_2Se_3$ bands and the projected $In_2Se_3$ bands in the contact system overlap with each other, as done in other similar works [32]. By measuring the energy difference between the conduction band minimum (CBM) and $E_F$, we can obtain the Schottky barrier height, which is 0.296 eV for the $P_\uparrow$ case and 0 eV for the $P_\downarrow$ case for this kind of interface. Thus, Schottky contact and Ohmic contact can be formed both at the Au-$In_2Se_3$ interface inside the lead and at the lead-channel interface, which jointly leads to the huge TER ratio.

Finally, we show that the difference in the contact distances between the two polarized states can be well explained by the different charge transfer between the two materials. After electrons transfer between Au(010) and the $In_2Se_3$ due to difference in work functions of them, an interface dipole is formed and Coulomb attractive interaction appears between the two materials. In the $P_\downarrow$ case, the electron transfer is much larger than that in the $P_\uparrow$ case and thus Coulomb attractive interaction is much stronger, which makes the contact distance much shorter (2.275 Å) than that (2.485 Å) in the $P_\uparrow$ case.

## IV. CONCLUSION

In conclusion, we have studied the electronic structure of the Au(010)-$In_2Se_3$ metal-semiconductor heterostructure and the electrical TER behavior of the FTJ constructed with Au(010)-$In_2Se_3$ as the leads and $In_2Se_3$ as the channel region. It is found that, after full structure relaxation, ferroelectricity of $In_2Se_3$ is still maintained even if it is in contact with Au(010) and two bistable states with different electric

polarization are obtained. Further, due to the zero tunnel barrier height, very good ability of electron injection is observed. More interestingly, it is found that the contact between Au and $In_2Se_3$ is of Schottky type when the direction of polarization of $In_2Se_3$ is towards Au(010). In contrast, it becomes Ohmic type when the direction of polarization is reversed. Further analysis indicates that it is caused by the difference of work functions on the two polar surfaces of $In_2Se_3$ and the subsequent substantially different charge transfer between Au(010) and $In_2Se_3$. The different contact types in the two polarized states lead directly to greatly different equilibrium tunnel conductances and ultimately a giant TER ratio more than $10^4\%$, which indicates that FTJs with metal contacts to 2D out-of-plane ferroelectric materials have a great potential of application in nonvolatile memory devices. Furthermore, two conditions of screening suitable metals for constructing FTJs with 2D FEMs may be suggested. One is the lattice mismatch between the 2D FEM and the metal, which should be as small as possible to reduce the strain-induced instability. The other condition is that the work function of the metal should be very close to one of the two work functions of the 2D FEM so that Schottky type and Ohmic type of contacts can be switched with the ferroelectric polarization reversal. These two contact types often result in two insulating and conducting states, which gives rise to large TER ratio. Of course, for FTJs with metal contacts, compared with all 2D FTJs, more factors should be taken into account due to the complex structure and bonding at the interfaces. For example, Fermi level pinning effect may also play an important role due to the metal-induced gap states, which are absent in all 2D FTJs with a van der Waals contact type [28]. Furthermore, another interesting fact to note is that if we control the polarization of the two leads separately so that the polarization directions in them are opposite, then a diode with good rectification performance may be achieved due to the asymmetrical structure.

[1] Z. Li, X. Guo, H.-B. Lu, Z. Zhang, D. Song, S. Cheng, M. Bosman, J. Zhu, Z. Dong, and W. Zhu, Adv. Mater. **26**, 7185 (2014).

[2] F. Ambriz-Vargas, G. Kolhatkar, M. Broyer, A. Hadj-Youssef, R. Nouar, A. Sarkissian, R. Thomas, C. Gomez-Yáñez, M. A. Gauthier, and A. Ruediger, ACS Appl. Mater. Inter. **9**, 13262 (2017).

[3] D. Kim, H. Lu, S. Ryu, C.-W. Bark, C.-B. Eom, E. Tsymbal, and A. Gruverman, Nano Lett. **12**, 5697 (2012).

[4] V. Garcia and M. Bibes, Nat. Commun. **5**, 4289 (2014).

[5] A. Chanthbouala, A. Crassous, V. Garcia, K. Bouzehouane, S. Fusil, X. Moya, J. Allibe, B. Dlubak, J. Grollier, S. Xavier *et al.*, Nat. Nanotechnol. **7**, 101 (2012).

[6] R. Soni, A. Petraru, P. Meuffels, O. Vavra, M. Ziegler, S. K. Kim, D. S. Jeong, N. A. Pertsev, and H. Kohlstedt, Nat. Commun. **5**, 5414 (2014).

[7] H. Lu, A. Lipatov, S. Ryu, D. Kim, H. Lee, M. Y. Zhuravlev, C.-B. Eom, E. Y. Tsymbal, A. Sinitskii, and A. Gruverman, Nat. Commun. **5**, 5518 (2014).

[8] V. S. Borisov, S. Ostanin, S. Achilles, J. Henk, and I. Mertig, Phys. Rev. B **92**, 075137 (2015).

[9] D. I. Bilc, F. D. Novaes, J. Iniguez, P. Ordejón, and P. Ghosez, ACS Nano **6**, 1473 (2012).

[10] L. L. Tao and J. Wang, Appl. Phys. Lett. **108**, 062903 (2016).

[11] K. Klyukin, L. L. Tao, E. Y. Tsymbal, and V. Alexandrov, Phys. Rev. Lett. **121**, 056601 (2018).

[12] A. Zenkevich, M. Minnekaev, Y. Matveyev, Y. Lebedinskii, K. Bulakh, A. Chouprik, A. Baturin, K. Maksimova, S. Thiess, and W. Drube, Appl. Phys. Lett. **102**, 062907 (2013).

[13] H. Lu, D. Lee, K. Klyukin, L. Tao, B. Wang, H. Lee, J. Lee, T. R. Paudel, L.-Q. Chen, E. Y. Tsymbal *et al.*, Nano Lett. **18**, 491 (2018).

[14] Z. Wen, C. Li, D. Wu, A. Li, and N. Ming, Nat. Mater. **12**, 617 (2013).

[15] J. D. Burton and E. Y. Tsymbal, Phys. Rev. Lett. **106**, 157203 (2011).

[16] Q. Yang, L. Tao, Y. Zhang, M. Li, Z. Jiang, E. Y. Tsymbal, and V. Alexandrov, Nano Lett. **19**, 7385 (2019).

[17] J. Junquera and P. Ghosez, Nature (London) **422**, 506 (2003).

[18] D. D. Fong, G. B. Stephenson, S. K. Streiffer, J. A. Eastman, O. Auciello, P. H. Fuoss, and C. Thompson, Science **304**, 1650 (2004).

[19] F. Xiong, X. Zhang, Z. Lin, and Y. Chen, J. Materiom. **4**, 139 (2018).

[20] A. I. Lebedev, J. Appl. Phys. **124**, 164302 (2018).

[21] R. Fei, W. Kang, and L. Yang, Phys. Rev. Lett. **117**, 097601 (2016).

[22] C. Xiao, F. Wang, S. A. Yang, Y. Lu, Y. Feng, and S. Zhang, Adv. Funct. Mater. **28**, 1707383 (2018).

[23] C. Liu, W. Wan, J. Ma, W. Guo, and Y. Yao, Nanoscale **10**, 7984 (2018).

[24] W. Ding, J. Zhu, Z. Wang, Y. Gao, D. Xiao, Y. Gu, Z. Zhang, and W. Zhu, Nat. Commun. **8**, 14956 (2017).

[25] C. Cui, W.-J. Hu, X. Yan, C. Addiego, W. Gao, Y. Wang, Z. Wang, L. Li, Y. Cheng, P. Li *et al.*, Nano Lett. **18**, 1253 (2018).

[26] L. Kang, P. Jiang, N. Cao, H. Hao, X. Zheng, L. Zhang, and Z. Zeng, Nanoscale **11**, 16837 (2019).

[27] X. Shen, Y.-W. Fang, B. Tian, and C.-G. Duan, ACS Appl. Electron. Mater. **1**, 1133 (2019).

[28] L. Kang, P. Jiang, H. Hao, Y. Zhou, X. Zheng, L. Zhang, and Z. Zeng, Phys. Rev. B **101**, 014105 (2020).

[29] I. Popov, G. Seifert, and D. Tománek, Phys. Rev. Lett. **108**, 156802 (2012).

[30] S. Das, H.-Y. Chen, A. V. Penumatcha, and J. Appenzeller, Nano Lett. **13**, 100 (2013).

[31] W. Liu, J. Kang, D. Sarkar, Y. Khatami, D. Jena, and K. Banerjee, Nano Lett. **13**, 1983 (2013).

[32] J. Kang, W. Liu, D. Sarkar, D. Jena, and K. Banerjee, Phys. Rev. X **4**, 031005 (2014).

[33] X. Zheng, A. Calò, E. Albisetti, X. Liu, A. S. M. Alharbi, G. Arefe, X. Liu, M. Spieser, W. J. Yoo, T. Taniguchi *et al.*, Nat. Electron. **2**, 17 (2019).

[34] Y. Wang, J. C. Kim, R. J. Wu, J. Martinez, X. Song, J. Yang, F. Zhao, A. Mkhoyan, H. Y. Jeong, and M. Chhowalla, Nature (London) **568**, 70 (2019).

[35] E. H. Rhoderick, IEE Proc. I: Solid-State Electron Dev. **129**, 1 (1982).

[36] K. Gong, L. Zhang, W. Ji, and H. Guo, Phys. Rev. B **90**, 125441 (2014).

[37] C. Gong, C. Huang, J. Miller, L. Cheng, Y. Hao, D. Cobden, J. Kim, R. S. Ruoff, R. M. Wallace, K. Cho *et al.*, ACS Nano **7**, 11350 (2013).

[38] Y. Pan, Y. Wang, M. Ye, R. Quhe, H. Zhong, Z. Song, X. Peng, D. Yu, J. Yang, J. Shi *et al.*, Chem. Mater. **28**, 2100 (2016).

[39] J. Kang, D. Sarkar, W. Liu, D. Jena, and K. Banerjee, in *Proceedings of the 2012 International Electron Devices Meeting* (IEEE, Piscataway, NJ, 2012), pp. 17–4.

[40] L. Bengtsson, Phys. Rev. B **59**, 12301 (1999).

[41] G. Kresse and J. Furthmüller, Phys. Rev. B **54**, 11169 (1996).

[42] G. Kresse and D. Joubert, Phys. Rev. B **59**, 1758 (1999).

[43] P. E. Blöchl, Phys. Rev. B **50**, 17953 (1994).

[44] J. P. Perdew, K. Burke, and M. Ernzerhof, Phys. Rev. Lett. **77**, 3865 (1996).

[45] S. Grimme, J. Comput. Chem. **27**, 1787 (2006).

[46] M. Brandbyge, J.-L. Mozos, P. Ordejón, J. Taylor, and K. Stokbro, Phys. Rev. B **65**, 165401 (2002).

[47] N. Papior, N. Lorente, T. Frederiksen, A. García, and M. Brandbyge, Comput. Phys. Commun. **212**, 8 (2017).

[48] D. Sánchez-Portal, P. Ordejon, E. Artacho, and J. M. Soler, Int. J. Quantum Chem. **65**, 453 (1997).

[49] J. M. Soler, E. Artacho, J. D. Gale, A. García, J. Junquera, P. Ordejón, and D. Sánchez-Portal, J. Phys.: Condens. Matter **14**, 2745 (2002).

[50] V. Heine, Phys. Rev. **138**, A1689 (1965).

[51] W. Chen, E. J. Santos, W. Zhu, E. Kaxiras, and Z. Zhang, Nano Lett. **13**, 509 (2013).

[52] C. Gong, L. Colombo, R. M. Wallace, and K. Cho, Nano Lett. **14**, 1714 (2014).

[53] W. Liu, W. T. Zheng, and Q. Jiang, Phys. Rev. B **75**, 235322 (2007).

[54] C. Chan, K. Ho, and K. Bohnen, in *Physical Structure*, edited by W. Unertl, Handbook of Surface Science, Vol. 1 (North-Holland, Amsterdam, 1996), pp. 101–136.